Detection of Graphene Cracks By Electromagnetic Induction, Insensitive to Doping Level

Taeshik Yoon[1, †], Sumin Kang[1, †], Tae Yeob Kang[1] and Taek-Soo Kim[1, 2, *]

Abstract: Detection of cracks is a great concern in production and operation processes of graphene based devices to ensure uniform quality. Here, we show a detection method for graphene cracks by electromagnetic induction. The time varying magnetic field leads to induced voltage signals on graphene, and the signals are detected by a voltmeter. The measured level of induced voltage is correlated with the number of cracks in graphene positively. The correlation is attributed to the increasing inductive characteristic of defective graphene, and it is verified by electromagnetic simulation and radio frequency analysis. Furthermore, we demonstrate that the induced voltage signal is insensitive to the doping level of graphene. Our work can potentially lead to the development of a high-throughput and reliable crack inspection technique for mass production of graphene applications.

1 Introduction

Defect is a significant obstacle to the use of chemical vapor deposited (CVD) graphene [Bae, Kim, Lee et al. (2010); Li, Cai, An et al. (2009); Reina, Jia, Ho et al. (2009)] in electronic devices. The superior characteristics of graphene such as high carrier mobility [Novoselov, Geim, Morozov et al. (2005)], mechanical strength [Lee, Wei, Kysar et al. (2008)] and thermal conductivity [Balandin, Ghosh, Bao et al. (2008)] are severely degraded by the presence of defects [Yazyev and Louie (2010); Zhu, Low, Perebeinos et al. (2012); Hwangbo, Lee, Kim et al. (2014); Zhang, Ma, Fan et al. (2014); Boutilier, Sun, O'Hern et al. (2014)]. The grain growth during the CVD process causes defects such as grain boundary, pinhole and vacancy at the atomic scale [Huang, Ruiz-Vargas, van der Zande et al. (2011); Kim, Lee, Regan et al. (2011); Duong, Han, Lee et al. (2012)]. The cracks, organic residues and wrinkles are frequently formed after the transfer of graphene [Kang, Shin, Bae et al. (2012)]. Among the various types of defects, crack is the one dimensional line defect ranges from few microns to few millimeters, but it becomes critical issues in two dimensional materials. The cracks in graphene block the electron transport increasing the electrical resistance. Moreover, the cracked graphene is unable to absorb

---

[1] Department of Mechanical Engineering, KAIST, Daejeon 34141, Korea.

[2] Graphene Research Center, KAIST, Daejeon 34141, Korea.

† These authors equally contributed to this work.

* Corresponding Author: Taek-Soo Kim. Email: tskim1@kaist.ac.kr.

enough strain energy, therefore, the mechanical strength is reduced. These issues substantially lower the performance and stability of soft electronics [Kim, Zhao, Jang et al. (2009); Lee, Kim, Jang et al. (2011)] which undergo severe mechanical deformation. Accordingly, after the transfer of graphene we should evaluate graphene defects, especially cracks, to ensure the uniform quality during the mass production of graphene applications.

Though there are many ways to inspect graphene defects, a high-throughput and doping insensitive crack inspection method is not demonstrated yet. The visualization of graphene defects was developed in various ways, because the optical detection of the defects is nearly impossible. By oxidation of metal substrate [Duong, Han, Lee et al. (2012); Yoon, Mun, Cho et al. (2014)] or reduction of metal ions [Ho, Liou, Chuang et al. (2015); Yoon, Kim, Choi et al. (2016); Park, Kim, Yoon et al. (2018)], defect sites are visible with metal oxides or metals. However, these are destructive methods by introduction of foreign materials, moreover the additional image conversion is required for the quantitative evaluation of defects. The Raman spectroscopy is also being used to evaluate graphene defects [Ferrari, Meyer, Scardaci et al. (2006); Cancado, Jorio, Ferreira et al. (2011)]. The atomic defects can be analyzed by the comparison of D and 2D peaks in the spectrum. However, the results give only limited information on the atomic-scale defects, and the micro-scale cracks should be inspected by the time-consuming area mapping. The easiest way for the evaluation of graphene defects is to measure the conductance of graphene [De and Coleman (2010)], because it reflects the degree of film integrity. In addition, the method for mapping the conductance of large-area graphene has been developed by using terahertz spectroscopy [Tomaino, Jameson, Kevek et al. (2011); Buron, Petersen, Boggild et al. (2012)]. Nevertheless, the testing is less reliable because of the conductivity change in graphene by chemical doping [Schedin, Geim, Morozov et al. (2007); Liu, Liu and Zhe (2011)].

In this work, we develop a high-throughput and reliable inspection method for graphene cracks based on electromagnetic induction. The number of cracks in graphene was evaluated by detecting induced voltage signals caused by time varying magnetic field. A defective graphene had a higher induced voltage peak than a non-defective one owing to increasing of self-inductance by introduced cracks. The self-inductance increasing was verified by electromagnetic simulation and radio frequency (RF) analysis. Moreover, we further demonstrated that the induced voltage signal was decoupled from chemical doping level of graphene.

2 Experimental details

Graphene specimen preparation: Synthesized graphene on Cu foil was attached to a thermal release tape, and the Cu foil was etched. The graphene on the thermal release tape was detached from the tape by heat treatment, and it was transferred onto a target substrate. The transferred graphene on a SiO_2/Si substrate was characterized by Raman spectroscopy to ensure the graphene layer is monolayer [Yoon, Shin, Kim et al. (2012)] (see Appendix A. Raman analysis of synthesized graphene). A 100-μm-thick PET substrate was cleaned in acetone, isopropyl alcohol, deionized water each for 5 min in an ultrasonic bath to remove contaminants on the surface, before transferring the graphene film.

Crack formation methods: Two crack formation methods, scratching and stretching, were exploited to investigate induced voltage signal with respect to the degree of damage. First, scratching cracks were formed with a cutting plotter (Jaguar IV, GCC Co., USA) on the center of the square and the strip types graphene-PET specimens, and the number of cracks was controlled from one to nine. The geometry and the dimension of the scratching cracks are represented in Appendix B. Second, stretching cracks were introduced by applying tensile strain on the strip type graphene-PET specimen with a high precision micromechanical test system (delaminator; DTS Company, Menlo Park, CA), and the amount of strain was controlled from 2.5% to 7.5%.

Graphene healing: Silver nitrate (AgNO$_3$) aqueous solution was prepared with a 10^{-3} M concentration for electrochemical deposition of silver ions on defect sites of graphene. The 7.5% strained graphene was immersed in the prepared solution and -2.5 V voltage was applied for 5 minutes.

3 Results and discussion

The inspection of graphene cracks was performed as follows (Fig. 1). First, a graphene specimen was placed on an electromagnet, and both ends of the specimen were contacted with electrical cables. The electromagnet and the electrical cables, which were contacted with graphene, were conneted with a signal generator and a voltmeter (Keithley 2000 Multimeter, Keithley Instruments), respectively. Second, the time-varying magnetic field was introduced by the electromagnet. The applied time-varying magnetic field generated electric current flow in the graphene specimen, and corresponding induced voltage was also generated. Third, the induced voltage signal in graphene was detected by the voltmeter. The number of cracks in graphene was evaluated by comparing induced voltage signals.
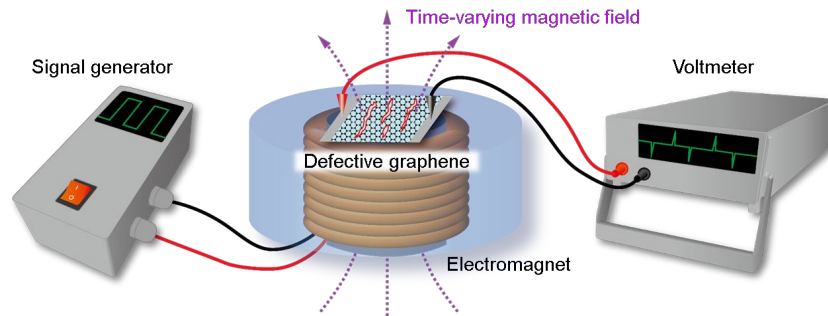
Figure 1: Schematic of the inspection method for graphene cracks by electromagnetic induction

Graphene specimens were prepared by integrating monolayer graphene on a polyethylene terephthalate (PET) substrate by using the conventional lamination-based transfer [Bae, Kim, Lee et al. (2010)] (see Experimental details section for graphene specimen preparation). We categorized the graphene specimens as two types namely, strip type and square type, because the inductance is dependent on geometry of specimens. The strip type specimen has 3×20 mm size (width and length respectively), and the square type

specimen has 10×10 mm size. Fig. 2(a) shows two types of specimen with respect to the number of cracks which were introduced by scratching with the cutting plotter (see Experimental details section for crack formation methods).

The prepared graphene specimens were placed on the electromagnet, and the time varying magnetic field was introduced by input of the signal generator. In this experiment, the electromagnet had 100-mm diameter and 60-mm length scale, but the size of electromagnet can be scaled up or down. Fig. 2(b) represents the input voltage profile of the signal generator which was controlled by switching the power. The applied magnetic field was rapidly changed when the switch was turned on or off. The rapidly changing magnetic field finally leads to induced voltage on the graphene specimen. Fig. 2(c) shows the measured induced voltage profiles of a pristine and a defective graphene. This result represents that the defective graphene has higher induced voltage peaks than the pristine graphene. Among the obtained peak values in each time varying magnetic field, we selected the highest peak value to evaluate the most accurate information for graphene cracks.
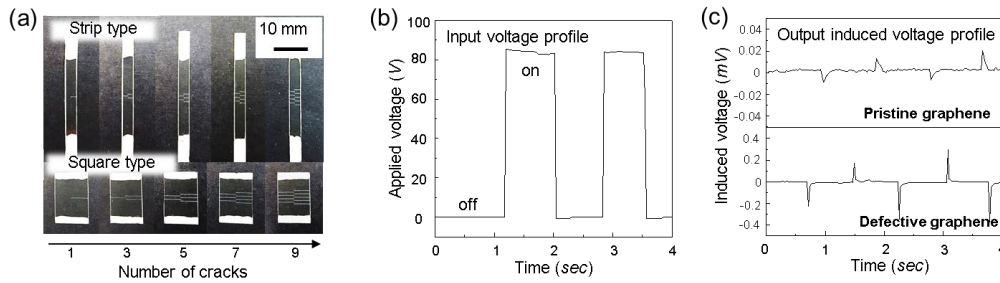
Figure 2: Prepared graphene specimens and voltage profiles. (a) The prepared strip and square typed graphene specimens with respect to the number of cracks. (b) The input voltage profile of the signal generator. The applied magnetic field is varied when the switch is turned on or off. (c) The detected output voltage profile by the voltmeter. A defective graphene has higher peak values of induced voltage than a pristine graphene

The peak induced voltage signals were characterized with respect to the number of cracks in graphene (Fig. 3(a)). The results indicate that the peak induced voltage is correlated with the number of cracks positively, because the crack increases self-inductance of graphene which depends on geometrical shape [Steinberg, Scheffler and Dressel (2010); Greenhouse (1974)]. Moreover, specimen length significantly influences on inductance of a thin conductive strip [Steinberg, Scheffler and Dressel (2010)]. For this reason, the strip type graphene specimens had a higher peak induced voltage than the square type specimens, over the whole range of the number of cracks.

For a more thorough inspection, we introduced micro-scale and large number of cracks by stretching strip type graphene-PET specimens (see Experimental details section for crack formation methods). The peak induced voltage which was measured on each strained specimen was plotted in Fig. 3(b). The peak induced voltage of the pristine specimen was 0.122±0.019 mV, while that of the 7.5% strained specimen was 1.420±0.021 mV. It means that the applied strain on graphene produced numerous cracks,

and it was reflected to the induced voltage. Furthermore, we performed selective defect healing of strained graphene by the electrochemical reduction of silver [Yoon, Kim, Choi et al. (2016)] (see Experimental Details section for graphene healing). The 7.5% strained graphene has the high induced voltage peak before healing. Whereas, the induced voltage peak decreased dramatically after healing, because defects in graphene were successfully closed and re-connected by silver ions (Fig. 3(c)). From these results, it was clarified that the induced voltage represents the degree of structural defects.
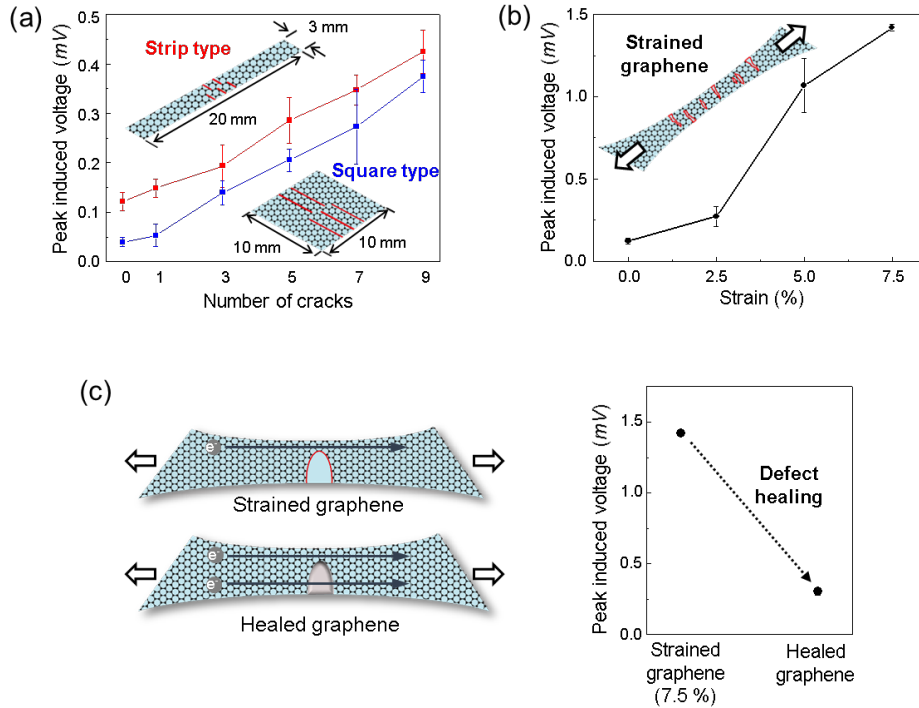
Figure 3: Correlation between graphene cracks and detected induced voltage signals. (a) Peak induced voltage of the strip type (red line) and the square type (blue line) graphene specimens with respect to the number of cracks. (b) Peak induced voltage of the strained graphene specimens. (c) Schematics and peak induced voltage of a strained and a healed graphene. The induced voltage signal decreases dramatically after selective healing of cracks

The induced voltage signal differences between a pristine and a defective graphene results from the self-inductance of graphene which depends on geometrical shape. To verify inductance variation of graphene, we performed finite element method (FEM) simulation and RF analysis. The scratched cracks, which were shown in Fig. 2(a), were modeled by commercial FEM software, COMSOL Multiphysics®. The air boundary was defined to confine magnetically permeable space, and static current was applied to calculate the inductance in cracked geometry. The calculated self-inductance is plotted in Fig. 4(a). In both specimen types, the graphene has higher inductance as the number of cracks increases. The obtained results indicate that graphene is electrically disconnected around cracks, and the cracks increase the inductance of films.

It has been observed that the scratched graphene has higher inductance than the non-defective graphene. Furthermore, the increased inductance on strained graphene was also verified by analyzing the RF response. In RF electronics, electrical properties such as inductance, capacitance and resistance are expressed by the scattering parameters. Especially, inductors in electrical circuits are characterized by the decrease in S21 parameters as frequency increases. We obtained the scattering parameters of the pristine and the strained graphene specimens using a network analyzer (Fig. 4(b)). In results, the graphs in S21 parameters of the 5% strained graphene specimen begin approximately 15 dB below one with the pristine specimen. Then, the S21 parameter of the strained specimen decreased more with increasing frequencies than that of the pristine specimen. The results show that the influence of cracks on inductance increasing of graphene, and correspond to the aforementioned experimental and FEM results.
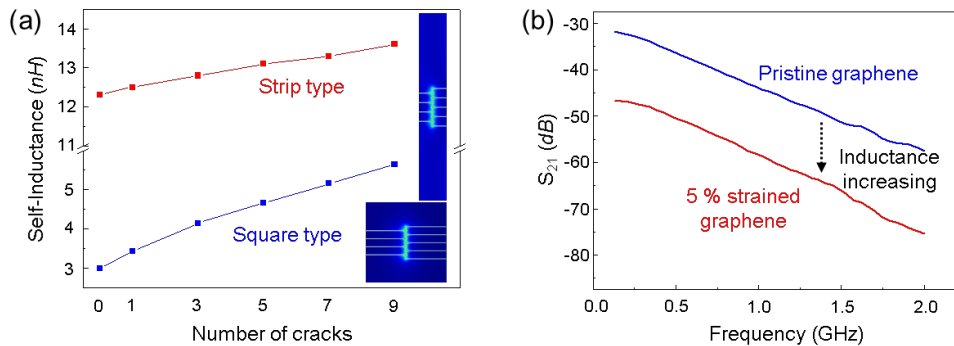
Figure 4: Role of crack on inductance of graphene. (a) Self-inductance of strip type (red line) and square type (blue line) graphene specimens with respect to the number of cracks, which is obtained by electromagnetic simulation. (b) Frequency response of the pristine and the strained graphene specimens. S12 parameters show that the 5% strained graphene has higher inductance than the pristine graphene

The measurement of electrical resistance is the easiest way to evaluate quality of graphene, however it has a critical drawback. The resistance is influenced by both geometric shape and electrical conductivity. The geometric shape is affected by the dimension of film and cracks, while the electrical conductivity of graphene is affected by surrounding environment such as chemical dopants, temperature, and humidity [Liu, Liu and Zhe (2011); Dan, Lu, Kybert et al. (2009)]. Therefore, the resistance measurement cannot ensure the reliable evaluation of graphene cracks. In this respect, the electromagnetic induction method ensures much reliable crack evaluation, because the inductance strongly depends on geometrical shape, and is independent to the electrical conductivity change [Steinberg, Scheffler and Dressel (2010)].

To investigate the influence of chemical doping on the electromagnetic induction method, we characterized both induced voltage and electrical resistance with respect to chemical doping level of graphene. The initially p-doped square type graphene specimens were used for experiments, and p-type and n-type dopants were introduced to graphene, respectively (Fig. 5(a)). For the p-type doping, graphene was immersed in a 0.05 M gold chloride

(AuCl3) aqueous solution for one minute. The change of induced voltage and resistance are plotted in Fig. 5(b). It was shown that the electrical resistance was significantly reduced by the p-type dopants on graphene, while the induced voltage was hardly changed. Moreover, n-type doping was induced on graphene by the electrolysis in DI water. Graphene was connected to cathode and -1 V was applied for 10 minutes, and the adsorption of hydrogen ions induced n-type doping on graphene [Ang, Chen, Wee et al. (2008)]. As shown in Fig. 5(c), the change of induced voltage was in the range of standard deviation while the resistance increased approximately 30%. These results indicate that the induced voltage signals are insensitive to the change of electrical conductivity.
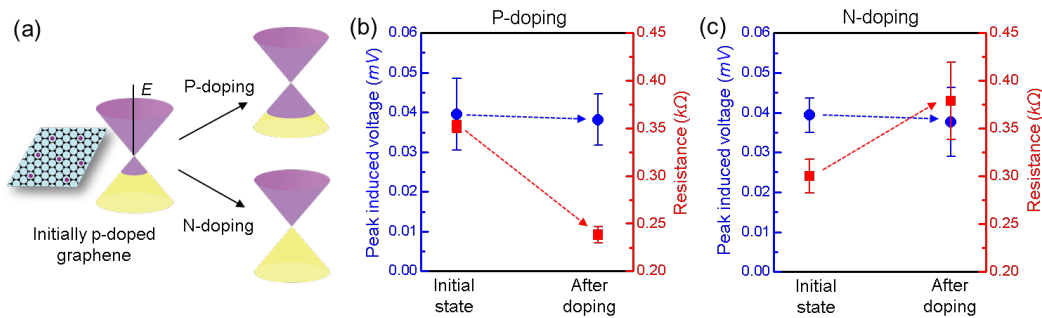
Figure 5: Characteristic of the electromagnetic induction method, insensitive to chemical doping level of graphene. (a) Schematic of doping induced Fermi level shifts of initially p-doped graphene. (b), (c) Peak induced voltage (blue points) and electrical resistance (red points) variations, when the p-type dopant (b) and the n-type dopant (c) are introduced to the initially p-doped graphene

4 Conclusion

In conclusion, the inspection method for graphene cracks was developed by the electromagnetic induction. The induced voltage, which represents the degree of structural defects, was generated on graphene by applying time-varying magnetic field, and detected by a voltmeter. The experimental results indicated that a defective graphene had a higher induced voltage peak than a pristine graphene due to inductance increasing which was verified by electromagnetic simulation and RF analysis. The obtained induced voltage was decoupled from the electrical conductivity change, therefore, reliable inspection of cracks was allowable. We expect that the proposed electromagnetic induction method would be utilized for a high-throughput inspection technology for mass production and operation of graphene based devices.

Notes: The authors declare no competing financial interest.

References

Ang, P. K.; Chen, W.; Wee, A. T. S.; Loh, K. P. (2008): Solution-gated epitaxial graphene as pH sensor. *Journal of American Chemical Society*, vol. 130, no. 44, pp. 14392-14393.

Bae, S.; Kim, H.; Lee, Y; Xu, X; Park, J. S. et al. (2010): Roll-to-roll production of 30-inch graphene films for transparent electrodes. *Nature Nanotechnology*, vol. 5, pp. 574-578.

Balandin, A. A.; Ghosh, S.; Bao, W.; Calizo, I.; Teweldebrhan, D. et al. (2008): Superior thermal conductivity of single-layer graphene. *Nano Letters*, vol. 8, no. 3, pp. 902-907.

Boutilier, M. S. H.; Sun, C.; O'Hern, S. C.; Au, H.; Hadjiconstantinou, N. G. et al. (2014): Implications of permeation through intrinsic defects in graphene on the design of defect-tolerant membranes for gas separation. *ACS Nano*, vol. 8, no. 1, pp. 841-849.

Buron, J. D.; Petersen, D. H.; Boggild, P.; Cooke, D. G.; Hilke, M. et al. (2012): Graphene conductance uniformity mapping. *Nano Letters*, vol. 12, no. 10, pp. 5074-5081.

Cancado, L. G.; Jorio, A.; Ferreira, E. H. M.; Stavale, F.; Achete, C. A. et al. (2011): Quantifying defects in graphene via raman spectroscopy at different excitation energies. *Nano Letters*, vol. 11, no. 8, pp. 3190-3196.

Dan, Y.; Lu, Y.; Kybert, N. J.; Luo, Z.; Johnson, A. T. C. (2009): Intrinsic response of graphene vapor sensors. *Nano Letters*, vol. 9, no. 4, pp. 1472-1475.

De, S.; Coleman, J. N. (2010): Are there fundmental limitations on the sheet resistance and transmittance of thin graphene films? *ACS Nano*, vol. 4, no. 5, pp. 2713-2720.

Duong, D. L.; Han, G. H.; Lee, S. M.; Gunes, F.; Kim, E. S. et al. (2012): Probing graphene grain boundaries with optical microscopy. *Nature*, vol. 490, pp. 235-239.

Ferrari, A. C.; Meyer, J. C.; Scardaci, V.; Casiraghi, C.; Lazzeri, M. et al. (2006): Raman spectrum of graphene and graphene layers. *Physical Review Letters*, vol. 97, no. 18, 187401.

Greenhouse, H. M. (1974): Design of planar rectangular microelectronic inductors. *IEEE Transaction on Parts, Hybrids, and Packaging*, vol. 10, no. 2, pp. 101-109.

Ho, P. H.; Liou, Y. T.; Chuang, C. H.; Lin, S. W.; Tseng, C. Y. et al. (2015): Self-crack-filled graphene films by metallic nanoparticles for high-performance graphene heterojunction solar cells. *Advanced Materials*, vol. 27, no. 10, pp. 1724-1729.

Huang, P. Y.; Ruiz-Vargas, C. S.; van der Zande, A. M.; Whitney, W. S.; Levendorf, M. P. et al. (2011): Grains and grain boundaries in single-layer graphene atomic patchwork quilts. *Nature*, vol. 469, pp. 389-392.

Hwangbo, Y.; Lee, C. K.; Kim, S. M.; Kim, J. H.; Kim, K. S. et al. (2014): Fracture characteristics of monolayer CVD-graphene. *Scientific Reports*, vol. 4, no. 4439.

Kang, J.; Shin, D.; Bae, S.; Hong, B. H. (2012): Graphene transfer: key for applications. *Nanoscale*, vol. 4, no. 18, pp. 5527-5537.

Kim, K. S.; Zhao, Y.; Jang, H.; Lee, S. Y.; Kim, J. M. et al. (2009): Large-scale pattern growth of graphene films for stretchable transparent electrodes. *Nature*, vol. 457, pp. 706-710.

Kim, K.; Lee, Z.; Regan, W.; Kisielowski, C.; Crommie, M. F. et al. (2011): Grain boundary mapping in polycrystalline graphene. *ACS Nano*, vol. 5, no. 3, pp. 2142-2146.

Lee, C.; Wei, X.; Kysar, J. W.; Hone, J. (2008): Measurement of the elastic properties and intrinsic strength of monolayer graphene. *Science*, vol. 321, no. 5887, pp. 385-388.

Lee, S. K.; Kim, B. J.; Jang, H.; Yoon, S. C.; Lee, C. et al. (2011): Stretchable graphene transistors with printed dielectrics and grate electrodes. *Nano Letters*, vol. 11, no. 11, pp. 4642-4646.

Li, X.; Cai, W.; An, J.; Kim, S.; Nah, J. et al. (2009): Large-area synthesis of high-quality and uniform graphene films on copper foils. *Science*, vol. 324, no. 5932, pp. 1312-1314.

Liu, H.; Liu, Y.; Zhe, D. (2011): Chemical doping of graphene. *Journal of Materials Chemistry*, vol. 21, no. 10, pp. 3335-3345.

Novoselov, K. S.; Geim, A. K.; Morozov, S. V.; Jiang, D.; Katsnelson, M. I. et al. (2005): Two-dimensional gas of massless Dirac fermions in graphene. *Nature*, vol. 438, pp. 197-200.

Park, I. J.; Kim, T. I.; Yoon, T.; Kang, S.; Cho, H. et al. (2018): Flexible and transparent graphene electrode architecture with selective defect decoration for organic light-emitting diodes. *Advanced Functional Materials*, vol. 28, no. 10, 1704435.

Reina, A.; Jia, X.; Ho, J.; Nezich, D.; Son, H. et al. (2009): Large area, few-layer graphene films on arbitrary substrates by chemical vapor deposition. *Nano Letters*, vol. 9, no. 1, pp. 30-35.

Schedin, F; Geim, A. K.; Morozov, S. V.; Hill, E. W.; Blake, P. et al. (2007): Detection of individual gas molecules adsorbed on graphene. *Nature Materials*, vol. 6, pp. 652-655.

Steinberg, K.; Scheffler, M.; Dressel, M. (2010): Microwave inductance of thin metal strips. *Journal of Applied Physics*, vol. 108, 096102.

Tomaino, J. L.; Jameson, A. D.; Kevek, J. W.; Paul, M. J.; van der Zande, A. M. et al. (2011): Terahertz imaging and spectroscopy of large-area single-layer graphene. *Optics Express*, vol. 19, no. 1, pp. 141-146.

Yazyev, O. V.; Louie, S. G. (2010): Electronic transport in polycrystalline graphene *Nature Materials*, vol. 9, pp. 806-809.

Yoon, T.; Kim, J. H.; Choi, J. H.; Jung, D. Y.; Park, I. J. et al. (2016): Healing graphene defects using selective electrochemical deposition: toward flexible and stretchable devices. *ACS Nano*, vol. 10, no. 1, pp. 1539-1545.

Yoon, T.; Mun, J. H.; Cho, B. J.; Kim, T. S. (2014): Penetration and lateral diffusion characteristics of polycrystalline graphene barriers. *Nanoscale*, vol. 6, no. 1, pp. 151-156.

Yoon, T.; Shin, W. C.; Kim, T. Y.; Mun, J. H.; Kim, T. S. et al. (2012): Direct

measurement of adhesion energy of monolayer graphene as-grown on copper and its application to renewable transfer process. *Nano Letters*, vol. 12, no. 3, pp. 1448-1452.

Zhang, P.; Ma, L.; Fan, F.; Zeng, Z.; Peng, C. et al. (2014): Fracture toughness of graphene. *Nature Communications*, vol. 5, no. 3782.

Zhu, W.; Low, T.; Perebeinos, V.; Bol, A. A.; Zhu, Y. et al. (2012): Structure and electronic transport in graphene wrinkles. *Nano Letters*, vol. 12, no. 7, pp. 3431-3436.

Appendix

A. Raman analysis of synthesized graphene

The Raman spectra of a transferred graphene on a SiO$_2$/Si substrate were analyzed to investigate the quality of the graphene film (Fig. (A1)). The arbitrary three points were characterized by irradiating the sample with a 514 nm laser beam. The inset photograph in the graph shows the transferred graphene on the substrate and the position of analyzed points. The G (~1580 cm^{-1}) and 2D (~2700 cm^{-1}) peak ratio represents that the synthesized graphene was a monolayer. Moreover, the small D peaks (~1350 cm^{-1}) indicate that the high-quality graphene was transferred on the target substrate.
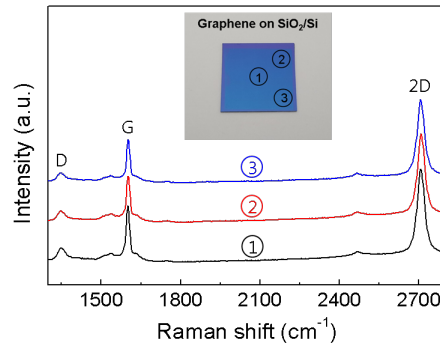
Figure A1: Raman spectra of a transferred graphene on a SiO$_2$/Si substrate

B. Dimension of scratching crack

The dimension of cracks which were introduced by scratching graphene-PET surface with cutting plotter was characterized by optical microscopy (Fig. (A2)). The length of cracks was determined with 1.5 mm and 5 mm for strip type and square type specimens respectively. The distance between cracks was controlled with 1 mm for both specimens, and each crack had 130 μm width.
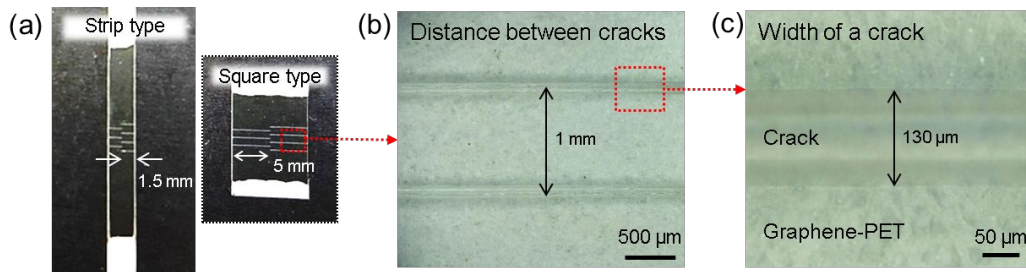
Figure A2: Dimension of scratching cracks; (a) length of cracks, (b) distance between cracks, and (c) width of a crack